

## High-cycle fatigue behavior of friction stir butt welded 6061 aluminium alloy

Hrishikesh DAS, Debayan CHAKRABORTY, Tapan KUMAR PAL

Welding Technology Centre, Metallurgical and Material Engineering Department,  
Jadavpur University, Kolkata-700032, India

Received 8 July 2013; accepted 12 October 2013

**Abstract:** Friction stir welding (FSW) of 6061 aluminium alloy butt joint was carried out at each rotation speed of 600, 800, 1000, 1200 r/min for two different travel speeds, 80 and 100 mm/min, at a constant probe depth of 1.85 mm. The calculated energy input based on the FSW parameters studied shows that the ultimate tensile strength (UTS) of the butt joint is obtained within a certain range of energy input of 297 kJ to 354 kJ out of total range of energy input studied from 196 kJ to 405 kJ. The fatigue behaviors of high-strength and low-strength joints performed at different stress ratios, i.e., 0.5, 0.3, 0.1,  $-0.3$ ,  $-0.5$ , indicate that the fatigue behaviors of both the welds are sensitive to the microstructural features, such as stir zone (SZ), thermo mechanically affected zone (TMAZ) and heat affected zone (HAZ). The observed fatigue strengths were discussed in terms of the microstructure, crack path behavior and fracture surface.

**Key words:** Al alloy; friction stir welding (FSW); high cycle fatigue; stress ratio ( $R$ -ratio); crack path

### 1 Introduction

Aluminium and aluminium alloys which are lighter weight and higher specific strength than ferrous material have found wide applications in recent years. The AA 6061 alloys are extensively used in marine frames, pipe lines, storage tanks and aircraft applications [1]. Although these alloys are readily weldable by fusion welding, they suffer from severe softening in the heat affected zone (HAZ) due to reversion of  $Mg_2Si$  precipitates during the welding thermal cycle. Such mechanical impairment presents a major problem in engineering design. In recent years, friction stir welding (FSW) has proven its capability as a commercial joining process for aluminium alloys. For example, in the aerospace industry, large tank for launch vehicles is being produced by FSW from high-strength aluminium alloys. In shipbuilding and rolling stock industries, the FSW process is exploited for the production of large prefabricated aluminium panels, which are made from aluminium extrusion.

In any structural design the fatigue behavior of welded joints continues to be an important factor. Several studies focusing on fatigue behavior of friction stir welded aluminium alloy joints with or without welding

flash have been reported [2–5]. ALI et al [5] observed that crack initiation was governed by stress concentration at the flash. However, it was opined that the microstructural effect on crack initiation probably overshadowed due to the presence of flash leading to stress concentration. To explore the microstructural aspect on fatigue behavior, ALI et al [5] conducted fatigue testing without flash and reported that fatigue crack nuclei were located within the nugget of friction stir welded 2024–T3 FS aluminium alloys. On the other hand, KAINUMA et al [4] showed that crack initiated in the parent material of A6N01 S–T6 FS welds. Furthermore, CAVALIERE et al [6] expressed that the effect of microstructure on the fatigue behavior of 6082–T6 weld is not clear. On precipitation hardened aluminium alloys, many investigators reported that fatigue life is affected by microstructure [7,8]. The fatigue crack growth resistance of peak aged aluminium alloys under constant amplitude testing was better than that of the overaged alloys, attributing to cyclic hardening caused by GP zones. On the optimized FSW process parameters for the maximum fatigue life in 5083–H321 aluminium alloy, LOMBARD et al [9] expressed that fatigue life is highly sensitive to influence on the crack initiation phase and to the existence of any easy growth routes in-plane with the fatigue crack.

Furthermore, they expressed that the optimum fatigue life requires both defect free-welds and frictional power input below about 1900 J/s derived from particular combination of tool feed rate and rotational speed.

So far fatigue behavior has been predominantly analyzed only for load in the tension region, i.e., at stress ratio  $R > 0$ . During actual service, many components are, however, subjected to both cyclic tensile stress and cyclic compressive stress, i.e., stress ratio  $R < 0$ . It is known from the literature that fatigue crack growth rate changes only insignificantly within the range of alternating tensile stress upto  $R = 0.5$  as compared to the results of tests normally conducted as  $R = 0$  to 0.1 [10]. However, there are very few publications relating to the effect of a combined tensile-compression load on fatigue behavior of FSW aluminium alloys. In addition, these are hardly comparable due to the difference in the material and the specimen analyzed.

In the present study, the fatigue behavior of FS welds of 6061–T6 aluminium alloys is investigated. Among eight combinations of FSW parameters studied, fatigue tests are conducted only for the maximum strength (rotation speed 1000 r/min, travel speed 80 mm/min) and minimum strength (rotation speed 600 r/min and travel speed 80 mm/min) achieved under tensile test, at stress ratio  $R = 0.3, 0.5, 0.1, -0.3$  and  $-0.5$  under axial loading. The influence of energy induced from different parameters combination on microstructure and fatigue behavior is discussed.

## 2 Experimental

The material used was 6061 aluminium sheet with 2.0 mm in thickness. The chemical compositions and mechanical properties of base metal are given in Table 1.

The base metals were cut into specimens of 300 mm × 100 mm for butt joint. All butt joints were produced using a RM series friction stir welder model RM1A–0.7. The machine can be operated with tool rotational speed up to 3000 r/min, axial load of 67 kN and plunge rates from 0.1 to 1000 mm/min. The axial force, torque and depth of penetration could be recorded simultaneously during each welding operation with the help of load cell coupled with a DAQ system. All the butt welds were made under displacement control mode.  $x$ -,  $y$ -,  $z$ -force and torque were recorded for each joint. The tool used was made of steel SKD61 and

comprised of a shank, shoulder (11 mm in diameter) and probe.

The tool axis was tilted by  $2^\circ$  with respect to the vertical axis of the plate surface and the depth of the probe tip was kept constant at 1.9 mm. Welding parameters such as rotation and travel speeds of the tool employed were varied and are listed in Table 2. The energy,  $Q$ , for FSW was calculated using the following expressions [11] and the energy values are summarized in Table 2.

$$Q = \int_0^t C_z(t) \times \frac{N_p \times 2\pi}{60} dt \quad (1)$$

where  $C_z$  and  $N_p$  represent torque and rotational speed, respectively;  $t$  is the ending time of welding.

The samples for metallographic studies were first cut and then polished using standard method and finally were etched with Keller's reagent (2 mL HF (48%)+ 3 mL HCl+5 mL HNO<sub>3</sub>+190 mL distilled H<sub>2</sub>O) to reveal the microstructure. Microstructural examination was carried out using a optical microscope (Make: Carl ZEISS; Model: Imager.A1m) and the microphotographs were taken at different magnifications. Microhardness measurements were performed on metallographically polished and etched samples across the butt joint from aluminium based metal through the different zones using Lica Vickers microhardness tester (Model: A–1170) at load 0.245 N (25 g) with dwell time 6 s and at an interval of 500  $\mu$ m. Transverse tensile specimens were cut from friction stir welded butt joint as per ASTM E8M–04. The tensile test was performed on a universal testing machine (INSTRON 8862) of 100 kN capacity at a cross head speed of 0.5 mm/min. High-cycle fatigue test was performed in a RUMUL made fatigue testing machine. Fracture surfaces of the tensile and fatigue fractured specimens were examined under JEOL JSM–8360 scanning electron microscope to understand the mode of fracture.

## 3 Results and discussion

### 3.1 Joint strength

The average ultimate tensile strength (UTS) of aluminium sheet joints under different combinations of rotational speed and traverse speed are summarized in Table 2. It is concluded from Table 2 that UTS could be achieved as high as 226 MPa, which is 77% that of base metal in butt joint of 6061 aluminium alloy by FSW. The

**Table 1** Chemical composition and mechanical properties of 6061 T6 base metal

Thickness/ mm	Chemical composition					Mechanical property	
	w(Si)/%	w(Mg)/%	w(Fe)/%	w(Cu)/%	w(Al)/%	YS/MPa	UTS/MPa
2	0.58	0.96	0.41	0.28	97.7	260	295

**Table 2** Parameter window and respective energy input

Rotation speed/ ( $r \cdot \text{min}^{-1}$ )	Travel speed/ ( $\text{mm} \cdot \text{min}^{-1}$ )	Energy/kJ	UTS/MPa
600	80	255	165
	100	196	171
800	80	292	177
	100	255	188
1000	80	354	226
	100	297	203
1200	80	405	195
	100	344	200

Depth of penetration: 1.9 mm

monotonic fracture locations have been created at the boundary between SZ and TMAZ on the advancing side in both 1000 r/min, 80 mm/min and 600 r/min, 80 mm/min treated specimens. Interestingly, tensile fracture occurred at or near the interface between stir zone and TMAZ on the advancing side of the joint. Similar fracture location after tensile testing of FSW aluminium alloys was also reported by LIU et al [12]. The remarkable difference in the structure particularly grain size between SZ and TMAZ has caused the fracture at or near the interface between the SZ and the TMAZ on the advancing side [13].

### 3.2 Correlation between weld pitch and energy and corresponding joint strength

It is interesting to note that the tensile strength increases significantly when the rotation speed increases from 600 r/min to 1000 r/min at a given traverse speed of 80 mm/min or 100 mm/min. In the case of 1200 r/min, at both the traverse speed of 80 mm/min and 100 mm/min the tensile strength decreases. This variation of tensile strength with rotational speeds for given traverse speed appears to be linked to the energy of the welds. Since increasing rotational speed results in increased heat generation (energy), since increasing traverse speed decreases heat generation, it is appropriate to use combined effect of rotational speed and traverse speed as measure of heat generation. Energy input vs welding speed plotted as shown in Fig. 1, which reveals the effect of two parameters on energy input and variation of tensile strength with energy input. Very high energy input (~405 kJ) leads to poor joint strength (~195 MPa) and very low energy input (~196 kJ) also shows poor joint strength (~171 MPa). Better joint strength as marked in Fig. 1 was achieved only within a certain range of energy input (297 kJ to 354 kJ). These show that energy has a significant effect on the microstructure and joint strength of 6061 aluminium alloy butt joint. It is worth

mentioning here that energy input has a strong correlation with residual stress distribution in the welds and there is a linear relationship with the maximum residual stress and energy input [9]. However, the residual stresses in the FSW welds are quite low due to the lower heat input and recrystallization accommodation of stresses. Thus, it is reasonable to believe that residual stress will contribute much less effect on performance of FSW welds.

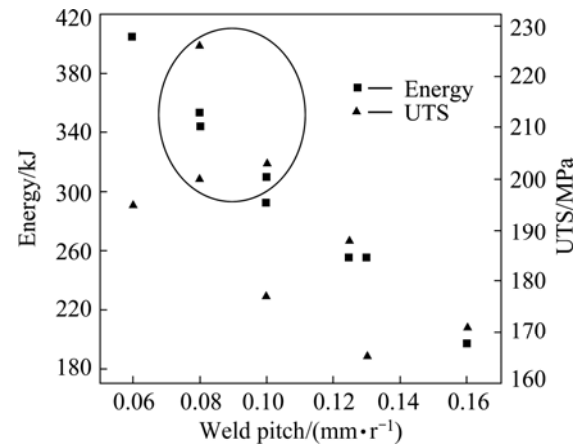


**Fig. 1** Energy input vs weld pitch (travel speed/rotation speed) and corresponding joint strength

### 3.3 Microstructures

The microstructures of the base metal and welds under parameters of (1000 r/min, 80 mm/min) and (600 r/min, 800 mm/min) treated specimens are shown in Figs. 2–4. The structures of the weld metal for all the joints have been classified into three regions: SZ, TMAZ and HAZ. The stir zone (Figs. 3(a) and 4(a)) consists of fine equiaxed grains due to dynamic recrystallization. Adjacent to the stir zone, the TMAZ (Figs. 3(b) and 4(b)) shows the severe deformation of grains due to the stirring action of the tool pin. It is evident that the welding parameters, especially rotation speed, affect the grain size in the stir zone of weld. The HAZ (Fig. 3(c) and

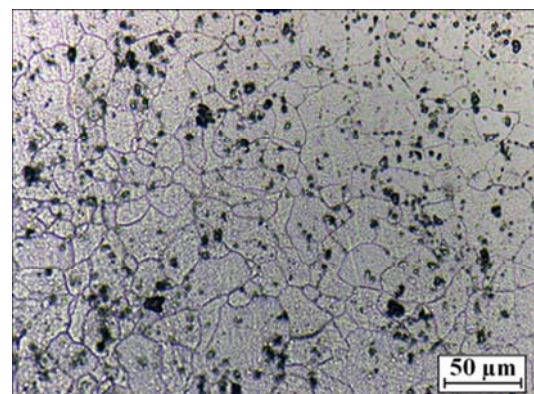


**Fig. 2** Microstructure of 6061 base metal

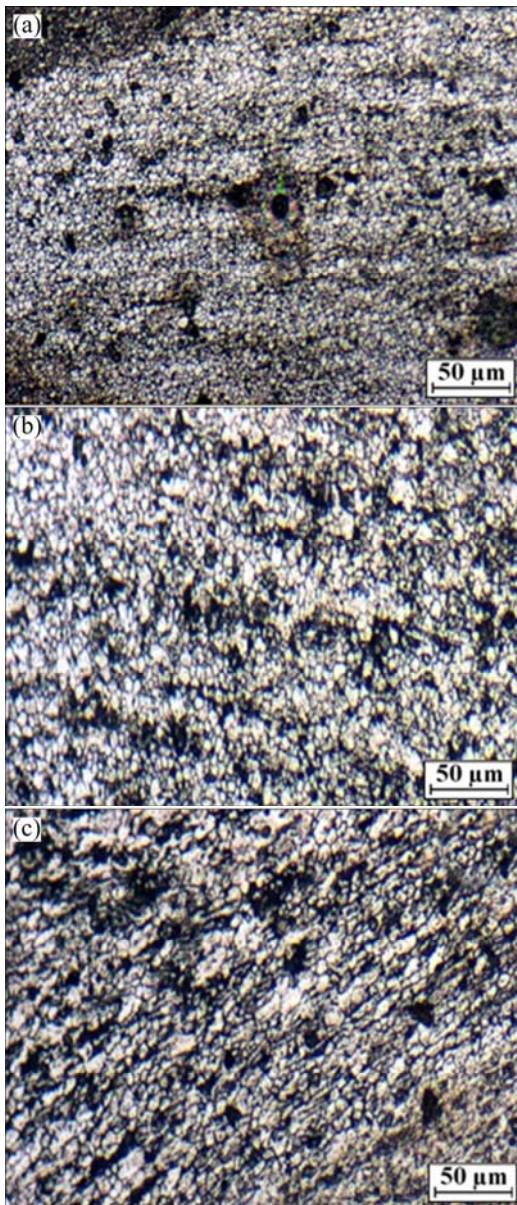


**Fig. 3** SEM images of recrystallized and equiaxed grains at SZ (a), TMAZ (b) and HAZ (c) of specimen under rotation speed of 600 r/min and travel speed of 80 mm/min

4(c)) shows finer grain than base metal. However, the elongated grains characteristic of the rolled base plate still exists. At a particular rotation speed, grain coarsening is significantly observed from SZ to TMAZ and then to HAZ. This is applicable for both the parameters studied. In TMAZ, the FSW tool has plastically deformed, in the material recrystallization did not occur and the heat from the adjacent zone resulted in coarser grain size compared to SZ. The HAZ is base metal affected by a thermal cycle only. Since peak temperature of the thermal cycle was not high, original microstructure of the base metal was modified by reheating process though the characteristic elongated grains of the rolled base plate could not be removed completely.

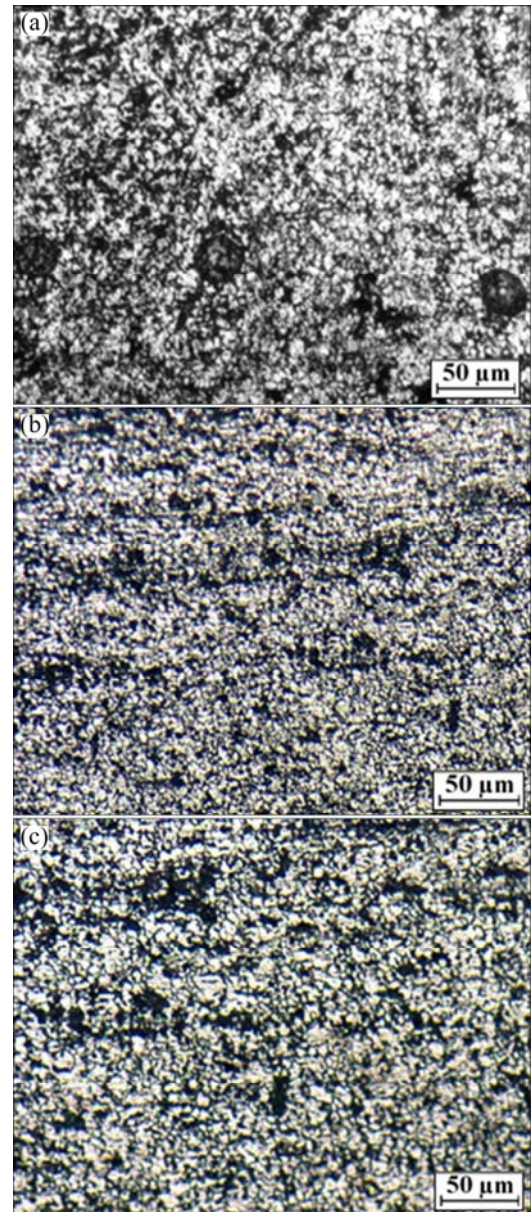


**Fig. 4** SEM images of recrystallized and equiaxed grains at SZ (a), TMAZ (b) and HAZ (c) of specimen under rotation speed of 1000 r/min and travel speed of 80 mm/min

The average grain sizes of the equiaxed grain in the SZ are about 4.5 and 7.65  $\mu\text{m}$  for welding parameters 1000 r/min, 80 mm/min and 600 r/min, 80 mm/min, respectively. The grains are severely deformed in the TMAZ which is the microstructural transition zone between SZ and HAZ. The mean grain sizes measured on the specimens in SZ, TMAZ, HAZ are shown in Fig. 5.

### 3.4 Microhardness profile

The Vickers microhardness profiles for the welds of 1000 r/min, 80 mm/min and 600 r/min, 80 mm/min are shown in Fig. 6. In both the welds, the hardness of the SZ is slightly lower than that of the parent metal. However, the hardness values for SZ, TMAZ and HAZ

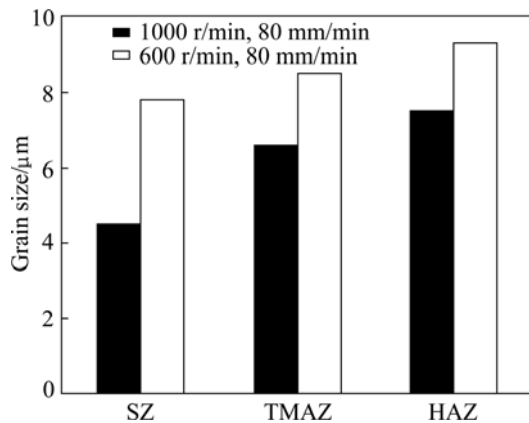


**Fig. 5** Grain size variation in SZ, TMAZ and HAZ for specimens obtained under 1000 r/min, 80 mm/min and 600 r/min, 80 mm/min

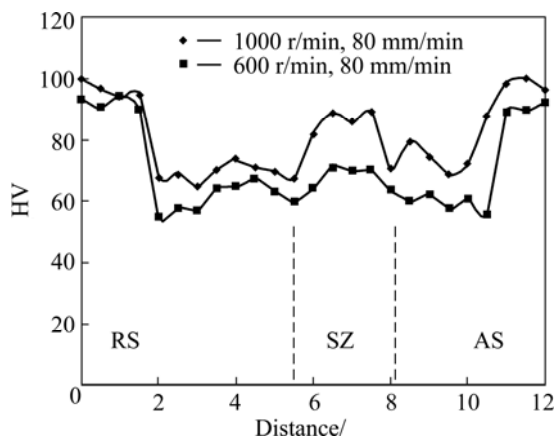


**Fig. 6** Microhardness plot for specimens obtained under 1000 r/min, 80 mm/min and 600 r/min, 80 mm/min

for specimens obtained under 1000 r/min, 80 mm/min are higher than those under 600 r/min and 80 mm/min. The peak hardness values are recognized in SZ compared to TMAZ and HAZ due to finer grains in SZ. The hardness minima are located at the HAZ. In fact, softening in the weld zone occurred and the low hardness plateau extended to the fine-grained area of SZ. This results suggest that dissolution of precipitate probably occurred in SZ and TMAZ and, therefore led to softening. In spite of finer grain size of HAZ compared to base metal, lower hardness observed in HAZ is believed to be due to over aging occurring during the FSW process.

### 3.5 Fatigue behavior

Figure 7 represents the stress–cycle (S–N) diagrams of the two welds obtained under parameters of (1000 r/min, 80 mm/min) and (600 r/min, 80 mm/min). It can be observed from Fig. 7 that in 6061 aluminium alloys, the weld obtained under (1000 r/min, 80 mm/min) has higher fatigue strength than weld obtained under (600

r/min, 80 mm/min), considering the fatigue limit defined as the fatigue strength at  $N=10^7$  cycles.

Fatigue fracture occurred at the boundary between SZ and TMAZ in the case of (600 r/min, 80 mm/min) treated specimen (Fig. 8). While fracture location

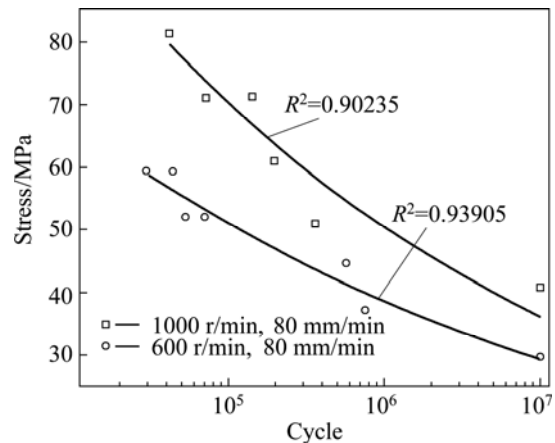


**Fig. 7** Stress–cycle curve of specimens at  $R=0.1$

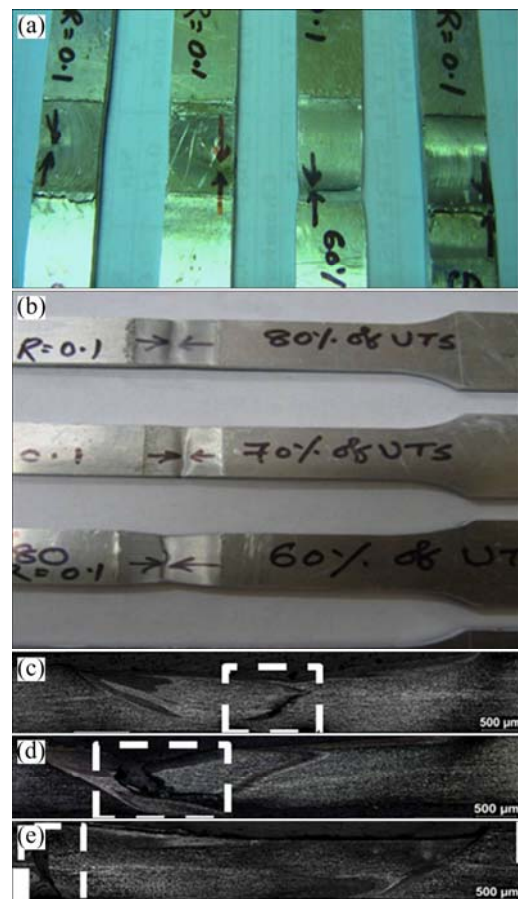


**Fig. 8** Fracture path for (600 r/min 80 mm/min) treated sample and fracture path shifting towards base metal of advancing side for (1000 r/min, 80 mm/min) treated sample: (a) 1000 r/min, 80 mm/min; (b) 600 r/min, 80 mm/min; (c) Stress amplitude 80%, 1000 r/min, 80 mm/min; (d) Stress amplitude 60%, 1000 r/min, 80 mm/min; (e) Stress amplitude 50%, 1000 r/min, 80 mm/min

changed with load applied in the case of (1000 r/min, 80 mm/min) treated specimen. At 80% stress amplitude, fatigue fracture occurred at the boundary between SZ and TMAZ. Whereas, at 60% and 50 % stress amplitude, fracture occurred at the boundary between TMAZ/HAZ and HAZ/BM, respectively. Such loading effect on fracture location is not observed in (600 r/min, 80 mm/min) treated specimen. However, it is interesting to note that fracture location remains unaltered (interface of SZ and TMAZ) for both the specimens with changing  $R$  ratio, although fatigue life decreased at  $R=-0.3$  and  $-0.5$ . The results of higher fatigue strengths associated with (1000 r/min, 80 mm/min) treated specimen as compared to (600 r/min, 80 mm/min) treated specimen suggest that microstructure with fine grains contributing higher UTS will exhibit better fatigue crack growth resistance than the microstructure having coarse grains. An important distinction between the two welds is that the average grain size in SZ for that the (1000 r/min, 80 mm/min) treated sample is  $4.5 \mu\text{m}$  and (600 r/min, 80 mm/min) treated sample is  $7.65 \mu\text{m}$ .

It should be noted that the dependence of fatigue life on grain size varies depending on the deformation mode. Grain size has the greatest effect on fatigue life in the low stress high-cycle regime in which stage I cracks predominate. Again, in high stacking fault energy (such as Al) cell structures develop readily, and these control stage I crack propagation [14].

For the small fatigue flaws considered in this work as a substantial part of the lifetime of real bodies consist of connecting and developing short cracks. The threshold stress [15] can be expressed as follows:

$$\sigma_{\text{th}} = \sigma_{\text{fr}}^* + \frac{K_C^m}{\sqrt{\pi w_0}} = \sigma_{\text{fr}}^* + \frac{K_C^m}{\sqrt{(\pi/2)d_g}} \quad (2)$$

where  $w_0$  is half the grain size  $d_g$ . In the present study, the grain size of sample obtained under 1000 r/min, 80 mm/min is smaller than that obtained under 600 r/min, 80 mm/min. The corresponding decrease in friction stress (which is equal to yield stress) for (1000 r/min, 80 mm/min) treated specimen compared to (600 r/min, 80 mm/min) treated specimen ( $\sim 10\%$ ) is not significant. Thus the threshold stress for small crack propagation in (1000 r/min, 80 mm/min) treated sample is expected to increase compared to (600 r/min, 80 mm/min) treated specimen.

In order to justify the perceived role of microstructural refinement on fatigue crack growth, the fractured ends of both (1000 r/min, 80 mm/min) treated and (600 r/min, 80 mm/min) treated samples were investigated with scanning electron microscope. Fatigue fracture for any microcrystalline ductile metal like

6061-T6 (Fig. 9) can be divided into three distinct zones. The crack initiation area (marked by black arrow in Fig. 9) is followed by zone *a* of stage I crack propagation, which is in turn followed by zone *b* of stage II crack propagation with prominent striation marks, and a final fracture zone *c* exhibits failure by void nucleation, coalescence and growth.

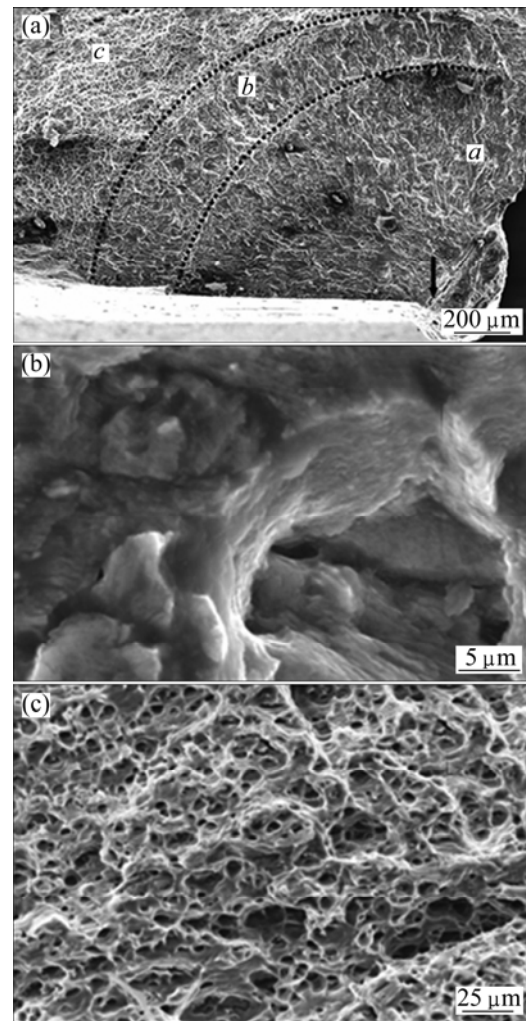


**Fig. 9** SEM images showing fracture surface at 80% of stress amplitude for (1000 r/min, 80 mm/min) treated sample at  $R=0.1$

Since stage I crack growth region extends only a few grain diameters [16], lower grain size of (1000 r/min, 80 mm/min) treated sample is associated with a much smaller extent of stage I crack growth compared to (600 r/min, 80 mm/min) treated sample. Furthermore, an increase in threshold stress for crack initiation (Eq. (2)) can encompass the effect of plastic crack closure on microscopic stress intensity. A detailed look at stage II crack propagation zone *b* in (600 r/min, 80 mm/min) treated sample shows prominent striation marks (Figs. 10(a) and (b)).

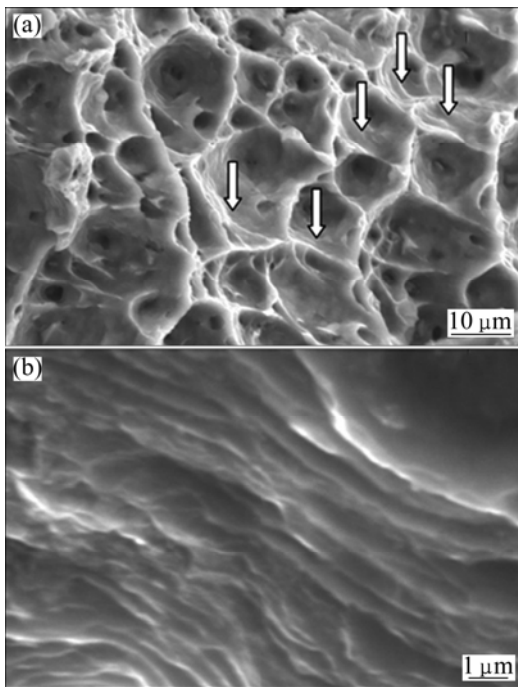


**Fig. 10** SEM images showing fracture surface with striation mark (a) and striation mark (b) at 80% of stress amplitude for specimen obtained under 600 r/min, 80 mm/min at  $R=0.1$

On the other hand, the striation marks in (1000 r/min, 80 mm/min) treated sample are shallow and less uniform (Fig. 9) compared to those in (600 r/min, 80 mm/min) treated sample. Considering the plastic blunting/resharpening model for striation formation by LAIRD [17], duplex slip is the primary criterion for striation formation in ductile face centered cubic materials. In coarse-grained (600 r/min, 80 mm/min) treated specimen, this would thus involve to and fro dislocation movement within grains. However, with decreasing grain size, dislocation movement becomes more difficult due to higher stress required to move them and the increase in interfacial area/volume leads to smaller planar slip distances. Thus striation formation in finer grains becomes more difficult, resulting in striation mark with a shallow and nonuniform spacing. Interestingly, crack deflection is much higher in the case of (1000 r/min, 80 mm/min) treated specimen compared to (600 r/min, 80 mm/min) treated one resulting from smearing of striation lines. Therefore, in (1000 r/min, 80 mm/min) treated specimen, it is expected that with increasing grain size from SZ to TMAZ, HAZ and base metal, the fracture path should shift towards the coarser grain size. However, the absence of such shifts of fracture path in (600 r/min, 80 mm/min) treated specimen is probably due to the very small difference in grain size among SZ, TMAZ and HAZ. Also, such crack deflection leads to a plastic closure effect which is

primarily responsible for improving the fatigue life. Furthermore, microhardness has been taken after fatigue test as shown in Fig. 11. Comparison between the hardnesses of two samples before and after fatigue test (under 50% of stress amplitude) clearly revealed that the hardness of base metal drastically decreased and the hardness of SZ drastically increased after fatigue test. Under cyclic loading, the hardened base metal became softer and softened SZ became work hardening.

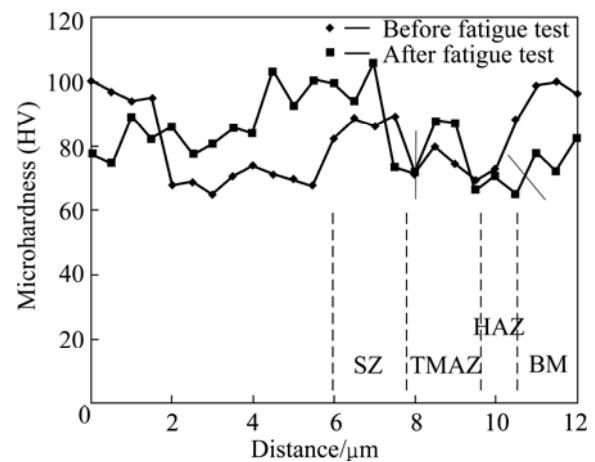


**Fig. 11** Comparison of microhardness before and after fatigue test (50% of stress amplitude) for (1000 r/min, 80 mm/min) treated specimen

In the present study, with the constant amplitude, 6061 aluminium FS welds in (1000 r/min, 80 mm/min) and (600 r/min, 80 mm/min) treated specimens,  $R$  ratio was changed, i.e.  $R=0.3, 0.5, -0.3$  and  $-0.5$ . It is interesting to note that fatigue life remains unaltered ( $10^7$ ) for both the specimens with changing  $R$  ratio ( $R=0.3, 0.5$ ) shown in Fig. 12(a). However, fatigue life of both the specimens drastically decreased at  $R=-0.3$  and  $-0.5$  shown in Fig. 12(b). The overall effect on total life was controlled primarily by the overload plastic zone immediately following the overload. The plastic zone size, however, can be drastically altered by subsequent cycling, particularly with negative  $R$  ratio [18]. Thus, the significance of the reversed stress plastic zone is subsequently reduced under subsequent negative  $R$  cycling. In general, fatigue crack striations could easily be depicted with a scanning electron microscope in the pre-overloaded region for all  $R$  values. However, with higher negative ratios, it becomes more difficult to find striations probably due to substantial abrasion and no microcracks have been observed (Figs. 13(a) and (b)). The experimental results, however, suggest that under spectrum loading conditions the negative portion of a loading spectrum cannot be neglected.

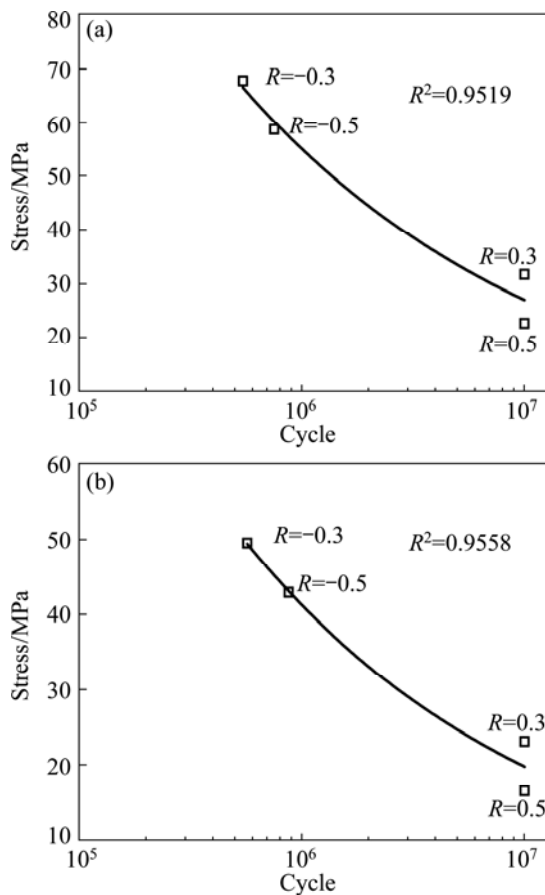


**Fig. 12** Stress–cycle curves for (1000 r/min, 80 mm/min) (a) and (600 r/min, 80 mm/min) (b) treated specimens at different  $R$  ratios

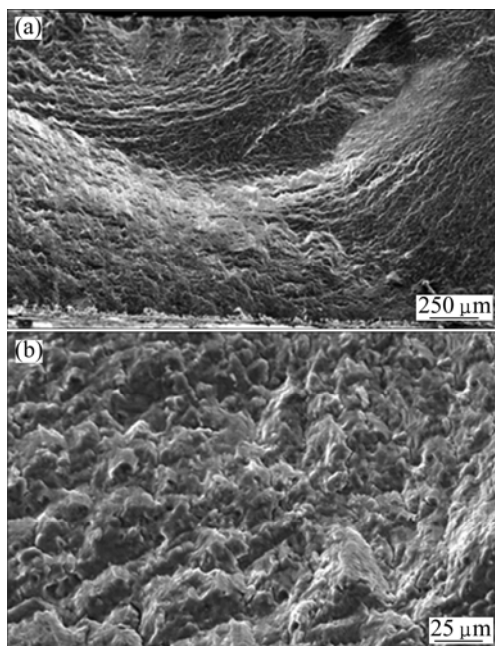


**Fig. 13** SEM images showing fracture surface of different zones (a) and microcracks (b) at  $R=-0.5$  for specimen obtained under 1000 r/min, 80 mm/min

## 4 Conclusions

1) Joint efficiency of FSW butt in relation to static strength of 6061 aluminium alloy base material was about 77%.

2) The fatigue strength at  $10^7$  cycles of FSW butt joint is about 40% of static strength (UTS). Further, improved fatigue strength was obtained at welding parameters of rotation speed 1000 r/min and travel speed 80 mm/min, indicating that the energy input has significant effect on fatigue behavior of welds.

3) The location of tensile and fatigue fracture was the same in the welds of (600 r/min, 80 mm/min) treated specimen and fracture occurred at the boundary between SZ and TMAZ. However, location of fatigue fracture was changed from the location of the tensile fracture in the welds of (1000 r/min, 80 mm/min) treated specimen. Furthermore, with decreasing load, location of fatigue fracture changed from the boundary between TMAZ and HAZ to the boundary between HAZ and base metal.

4) Fatigue test performed at different  $R$  ratios shows that at the constant stress (at  $10^7$ ), fatigue life remains unaltered ( $10^7$ ) for the specimens at  $R=0.3$  and  $0.5$ , but drastically decreases for the specimens at  $R=-0.3$  and  $-0.5$ .

## References

- [1] STALEY J T. Aluminum-based products for the aerospace industry produced using non-traditional processing [C]//First International Conference on Processing Materials for Properties. Honolulu, Hawaii, USA: The Minerals, Metals and Materials Society (TMS), 1993.
- [2] ERICSSON M, SANDSTRÖM R. Influence of welding speed on the fatigue of friction stir welds, and comparison with MIG and TIG [J]. *Int J Fatigue*, 2003, 25(12): 1379–1387.
- [3] LOMOLINO A S, TOVOB R, SANTOS J. DOS on the fatigue behaviour and design curves of friction stir butt-welded Al alloys [J]. *Int J Fatigue*, 2005, 27(3): 305–316.
- [4] KAINUMA S, KATSUKI H, IWAI I, KUMAGAI M. Evaluation of fatigue strength of friction stir butt-welded aluminum alloy joints inclined to applied cyclic stress [J]. *Int J Fatigue*, 2008, 30(5): 870–876.
- [5] ALI A, AN X, RODOPOULOS C A, BROWN M W, HARA P O', LEVERS A. The effect of controlled shot peening on the fatigue behaviour of 2024-T3 aluminium friction stir welds [J]. *Int J Fatigue*, 2007, 29(8): 1531–1545.
- [6] CAVALIERE P, SQUILLACE A, PANELLA F. Effect of welding parameters on mechanical and microstructural properties of AA6082 joints produced by friction stir welding [J]. *J Mater Process Technology*, 2008, 200: 364–372.
- [7] JATA K V, SANKARAN K K, RUSCHAU J J. Friction-stir welding effects on microstructure and fatigue of aluminum alloy 7050-T7451 [J]. *Metall Mater Trans A*, 2000, 31: 2181–2192.
- [8] SU J Q, NELSON T W, MISHRA R, MAHONEY M. Microstructural investigation of friction stir welded 7050-T651 aluminium [J]. *Acta Mater*, 2003, 51(3): 713–729.
- [9] LOMBARD H, HATTINGH D G, STEUWER A, JAMES M N. Optimising FSW process parameters to minimize defects and

- maximize fatigue life in 5083-H321 aluminium alloy [J]. International Journal of Engineering Fracture Mechanics, 2008, 75: 341–354.
- [10] HUANG X P, MOAN T. Improved modeling of the effect of  $R$ -ratio on crack growth rate [J]. International Journal of Fatigue, 2007, 29: 591–602.
- [11] ZIMMER S, LANGLOIS L, LAYE J, BIGOT R. Experimental investigation of the influence of the FSW plunge processing parameters on the maximum generated force and torque [J]. Int J Adv Manuf Technol, 2010, 47: 201–215.
- [12] LIU H J, FUJII H, MAEDA M, NOGI K. Tensile properties and fracture locations of friction stir-welded joints of 2017 T351 aluminum alloy [J]. Journal of Materials Processing Technology, 2003, 142: 692–696.
- [13] GUPTA R, DAS H, PAL T K. Influence of processing parameters on induced energy, mechanical and corrosion properties of FSW butt joint of 7475 AA [J]. Journal of Material Engineering and Performance, 2012, (DOI) 10.1007/s11665-011-0074-2.
- [14] DIETER E G. Mechanical Metallurgy [M]. London: McGraw-Hill Book Company, 1988: 417–419.
- [15] TANAKA K, NAKAI Y, YAMASHITA M. Fatigue growth threshold of small cracks [J]. Int J Fracture, 1981, 17: 519–533.
- [16] MILLER K J. Materials science perspective of metal fatigue resistance [J]. Mat Sci Tech, 1993, 9: 453–462.
- [17] LAIRD C. The influence of metallurgical structure on the mechanisms of fatigue crack propagation [C]//STP 415, American Society for Testing and Materials, 1976: 415.
- [18] STEPHENS R I, CHEN D K, HOM B W. Fatigue crack growth with negative stress ratio following single overloads in 2024-T3 and 7075-T6 aluminum alloys [C]//Fatigue Crack Growth Under Spectrum Loads, ASTM STP 595. Philadelphia: American Society for Testing and Materials, 1976: 27–40.

## 搅拌摩擦对接焊 6061 铝合金的高周疲劳行为

Hrishikesh DAS, Debayan CHAKRABORTY, Tapan KUMARPAL

Welding Technology Centre, Metallurgical and Material Engineering Department,  
Jadavpur University, Kolkata-700032, India

**摘要:** 对 6061 铝合金进行搅拌摩擦对接焊, 其焊接工艺参数为: 旋转速度 600、800、1000、1200 r/min, 前进速度 80、100 mm/min, 探针插入深度 1.85 mm。基于搅拌摩擦焊参数计算得到的能量输入结果表明, 在输入能量为 196~405 kJ 的情况下, 接头在 297~354 kJ 的输入能量范围内有最大的抗拉强度。在不同的应力比( $R=0.5, 0.3, 0.1, -0.3, -0.5$ )下, 将高强度、低强度 2 种焊接头进行疲劳测试。结果表明, 对于这 2 种焊接头, 显微组织特征明显影响其疲劳性能, 比如搅拌区、热力影响区(TMAZ)和热影响区。从接头的显微组织、裂纹扩展路径和断裂表面观察等方面对其疲劳强度进行讨论。

**关键词:** 搅拌摩擦焊; 高周疲劳; 应力比; 裂纹路径

(Edited by Hua YANG)